Editors' Suggestion

Characterizing vortex tangle properties in steady-state He II counterflow using particle tracking velocimetry

Brian Mastracci and Wei Guo*

National High Magnetic Field Laboratory, 1800 E Paul Dirac Drive, Tallahassee, Florida 32310, USA and Department of Mechanical Engineering, Florida State University, 2525 Pottsdamer Street, Tallahassee, Florida 32310, USA

(Received 31 October 2018; published 7 February 2019)

Historically, there has been little faith in particle tracking velocimetry (PTV) as a tool to make quantitative measurements of thermal counterflow in He II, since tracer particle motion is complicated by influences from the normal fluid, superfluid, and quantized vortex lines, or a combination thereof. Recently, we introduced a scheme for differentiating particles trapped on vortices (G1) from particles entrained by the normal fluid (G2). In this paper, we apply this scheme to demonstrate the utility of PTV for quantitative measurements of vortex dynamics in He II counterflow. We estimate ℓ, the mean vortex line spacing, using G2 velocity data, and c_2, a parameter related to the mean curvature radius of vortices and energy dissipation in quantum turbulence, using G1 velocity data. We find that both estimations show good agreement with existing measurements that were obtained using traditional experimental methods. This is of particular consequence since these parameters likely vary in space, and PTV offers the advantage of spatial resolution. We also show a direct link between power-law tails in transverse particle velocity probability density functions (PDFs) and reconnection of vortex lines on which G1 particles are trapped.

DOI: 10.1103/PhysRevFluids.4.023301

I. INTRODUCTION

Whole field flow visualization has become a popular research tool for He II [1], the superfluid phase that occurs in ^{4}He at temperatures below about 2.17 K. One common visualization method, particle tracking velocimetry (PTV), tracks the locations of individual micron-sized solidified hydrogen or deuterium tracer particles suspended in the flow field throughout a sequence of photographs. It is trivial to obtain an ensemble of velocity measurements from these time-resolved sequences of particle locations, which can be used, in theory at least, to characterize quantitatively the fluid behavior.

In practice, extraction of reliable, quantitative information from particle velocity measurements has been elusive due to the nonclassical mechanics of He II. The two-fluid model of Tisza and Landau describes it as two interpenetrating and fully miscible fluid components [2,3]. The normal fluid behaves more or less classically, and saturates the He II system at the phase transition temperature $T_\lambda \approx 2.17$ K. It entrains tracer particles by viscous drag. The superfluid component, which saturates the two-fluid system below about 1 K, is inviscid and carries no entropy, but still influences particle motion through inertial and added mass effects [4]. Furthermore, circulation in the superfluid is confined to quantized vortex lines, each with a single quantum of circulation $\kappa \approx 10^{-8}$ m^2/s about a core $\xi_0 \approx 0.1$ nm in diameter. Pressure gradients in the vicinity of each

*Author to whom correspondence should be addressed: wguo@magnet.fsu.edu

vortex line can attract and trap particles [5,6], though, once trapped, they have a tendency to slide along the vortex core under the influence of drag exerted by the normal fluid [7,8].

Application of PTV to He II becomes increasingly complicated in studies of thermal counterflow, a heat transfer mechanism unique to He II. In response to a thermal stimulus, the normal fluid carries entropy away from the heat source with velocity v_n proportional to the heat flux q, while the superfluid moves toward it at v_s such that there is no net mass transfer. As q increases the two fluids can become independently turbulent [9]. Turbulence in the superfluid manifests as a random tangle of quantized vortex lines [10], and a nonclassical form of turbulence arises in the normal fluid [9] due to a force of mutual friction that arises from interactions with the vortex tangle [11].

Since tracer particles interact with both fluid components, a major challenge when applying PTV to thermal counterflow is determining what influences the motion of an observed particle at a given time, so that the behavior of the underlying flow field can be interpreted correctly [9,12–14]. Until recently analysis was confined to qualitative characterizations: evolution of particle motion in response to applied heat flux [15], or of statistical distributions of particle kinematics in response to image acquisition rate [16,17]. A newer visualization technique employing metastable He_2^* excimers as tracer particles avoids this ambiguity issue, since the eximers are not trapped on vortices above about 1 K [14]. However, as a compromise, information about the vortex dynamics cannot be obtained, and thus far this method yields information about the flow velocity in one dimension only.

Recently, we studied particle motion in thermal counterflow across a wide heat flux range using PTV, and found that, indeed, particles moving under the influence of relatively high heat flux, to which we give the name G3, are constantly affected by both the normal fluid and vortex lines [18,19]. However, for relatively low heat flux, we devised a scheme for analyzing the kinematics of particles entrained by the normal fluid, to which we give the name G2, separately from those trapped on vortices, which we call G1 [20]. Using this separation scheme, we proposed a simple estimation of the mean free path of G2 particles through the vortex tangle, we showed that G1 velocity fluctuations are likely caused by fluctuations of the local vortex line velocity, and we showed that power-law tails in transverse particle velocity probability density functions (PDFs) are due entirely to G1. In the present paper, we expand upon these ideas, with a focus on demonstrating the utility of PTV for quantitative analysis of the vortex tangle. After a brief overview of the experimental apparatus and data analysis scheme in Sec. II, we motivate, present, and discuss each main result in its own section. An experimental estimation of the mean vortex line spacing using flow visualization is presented in Sec. III. An experimental estimation of c_2, a parameter related to energy dissipation in quantum turbulence [21], is presented in Sec. IV. A direct link between vortex line reconnection and G1 transverse velocity PDF power-law tails is established in Sec. V. We conclude in Sec. VI.

II. EXPERIMENTAL PROTOCOL

This work employs the same apparatus, illustrated in Fig. 1, described in our previous papers [20,22]. Solidified deuterium tracer particles with mean diameter $d_p \approx 4.6\ \mu$m are delivered via stainless steel tube to the center of a $1.6 \times 1.6 \times 33$ cm^3 vertical flow channel immersed in a saturated He II bath. The delivery tube is then retracted by an external electric motor, and a 400 Ω planar resistive heater at the bottom of the channel generates thermal counterflow. A laser beam with cross section approximately 200 μm thick and 9 mm tall illuminates particles as they move through the geometric center of the channel, and a high-speed digital camera captures them on video. A modified feature point tracking algorithm [23] yields the position of each particle in each video frame, information that can be readily transformed into velocity measurements for each particle.

Our data set covers three temperatures, $T = 1.70$, 1.85, and 2.00 K, with heat currents ranging from 29 to 481 mW/cm^2. Figure 2 shows (a) streamwise and (b) transverse particle velocity PDFs typical of PTV measurements in thermal counterflow driven by relatively low heat flux. In the streamwise PDFs, one peak arises from G1, the name we give to particles trapped on quantized vortices, and the other from G2, the name we give to particles entrained by the normal fluid. To

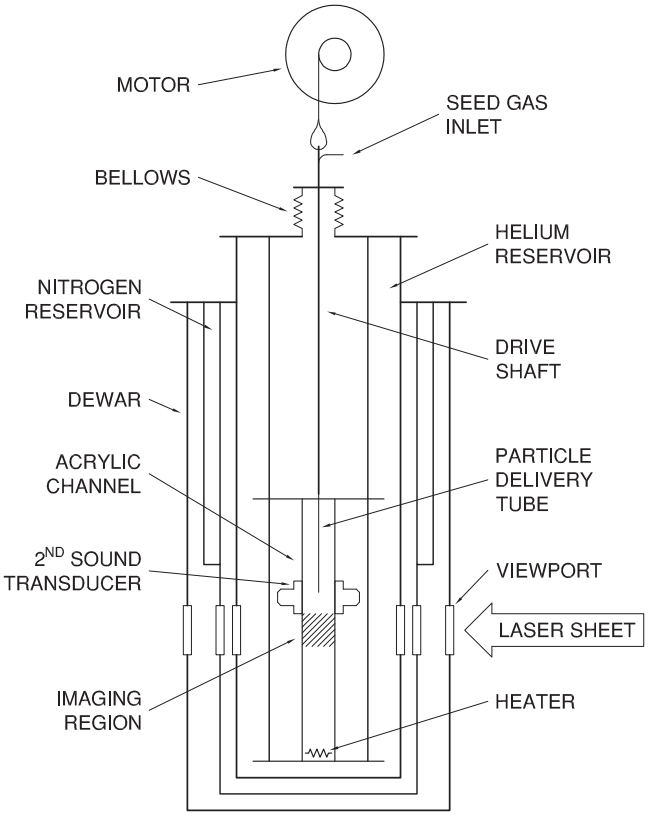

FIG. 1. Simple illustration of the experimental apparatus (not to scale).

determine the category to which a velocity measurement v_p contributes, we apply the following criteria [20]. If $v_p < \mu_2 - 2\sigma_2$, where μ_2 and σ_2 are the mean and standard deviation, respectively, of the G2 peak, then v_p exhibits G1 behavior. If $v_p > \mu_1 + 2\sigma_1$, then v_p exhibits G2 behavior. In the event that the peaks are well separated, i.e., $\mu_2 - \mu_1 > 2(\sigma_1 + \sigma_2)$, the criteria are reversed. The separation scheme results in ensembles of velocity measurements representing G1 and G2, which can be used for further analysis, including generation of the transverse PDFs of Fig. 2(b), which are normalized by standard deviation. It can be seen that a Gaussian curve, indicated by the solid black line, fits the core of the G1 PDF and the entirety of the G2 PDF. Beyond about four standard deviations from the center, a power-law curve ($\propto |u_p|^{-3}$), indicated by the dashed black line, passes through the tail of the G1 PDF.

In addition to PTV, we employ second sound attenuation to measure the average vortex line length per unit volume, or vortex line density L, inside the channel. As a consequence of the two fluid model, He II supports multiple speeds of sound, including second sound, the wavelike propagation of temperature or entropy. A pair of second sound transducers, as illustrated in Fig. 1, establish a standing second sound wave across the channel that is attenuated in the presence of quantized vortices, and the vortex line density can be obtained from the degree of attenuation [24].

III. MEAN FREE PATH AND VORTEX LINE DENSITY

To explain the underlying mechanism that governs whether particles exhibit G1 or G2 behavior, we acknowledged that, at the beginning of each video acquisition, some particles are already trapped on vortices (G1) while others are not (G2). Untrapped particles then move over a distance

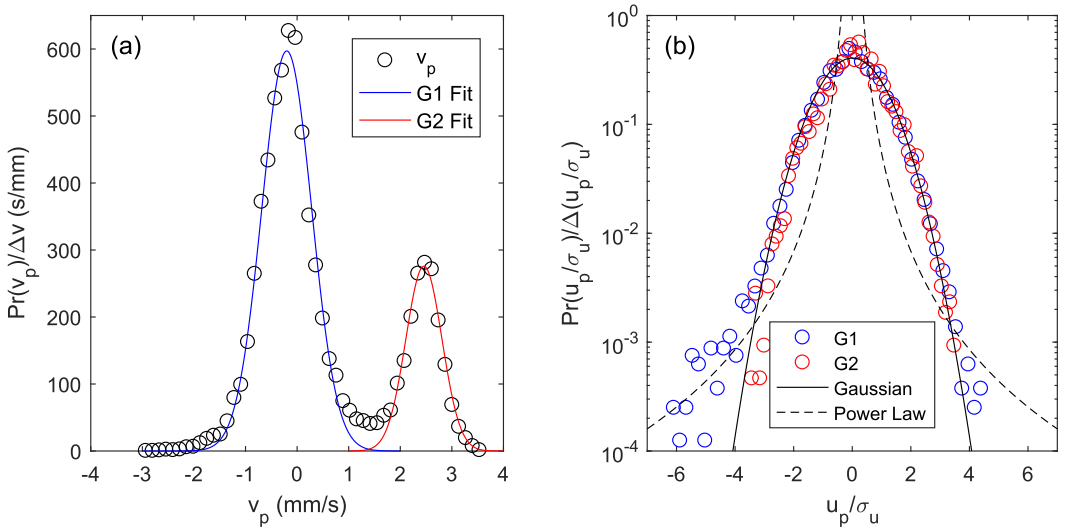

FIG. 2. Typical (a) streamwise velocity PDF ($T = 1.85$ K, $q = 38$ mW/cm^2) and (b) transverse velocity PDFs ($T = 2.00$ K, $q = 113$ mW/cm^2) obtained from PTV measurements of thermal counterflow at relatively low heat flux. The transverse velocity PDFs are normalized by standard deviation σ_u.

comparable to their mean free path s through the vortex tangle. We proposed that a particle becomes trapped if the vortex line length enclosed within the volume defined by its mean free path and trapping cross section is comparable to the diameter of the cross section. Approximating the trapping cross section as the two-dimensional projection of the particle, $\pi d_p^2/4$, we obtained the relationship

$$s \leqslant \frac{4}{\pi d_p L}, \tag{1}$$

and showed that, qualitatively, the mean free path predicted by this simple model agrees with the length of observed G2 tracks [20]. To explore the usefulness of this model, we will accept its validity, and use Eq. (1) to estimate the mean vortex line spacing $\ell = L^{-1/2}$ by using the length of G2 tracks to represent s.

We first recognize that, for 2D planar velocimetry, G2 tracks begin and end for reasons other than detrapping or trapping events. Particles tracing the normal fluid are free to enter and leave the imaging plane through the top or bottom of the image. They may also drift in or out of plane in the direction normal to the camera due to minor imperfections, such as misalignment or vibrations, in the experimental apparatus. As a result, many observed tracks are likely shorter than the mean free path. It is therefore inappropriate to assume that the mean G2 track length accurately represents s. Alternatively, since it is not possible to observe a track longer than the mean free path (at least, not much longer), we estimate it with the mean length of the longest 10% of observed G2 tracks.

Figure 3 shows the mean vortex line spacing as a function of heat flux for (a) 1.70 K, (b) 1.85 K, and (c) 2.00 K. Red markers predict ℓ using Eq. (1), where the longest 10% of G2 tracks observed for each point in the parameter space represent s and $d_p = 4.6 \pm 1.3$ μm [22]. Blue markers represent the line spacing obtained from traditional second sound attenuation.

For a simple approximation, the accuracy is remarkable; in many cases, the line spacing measured using PTV falls within one standard deviation (indicated by the error bars) of the line spacing measured using second sound. This suggests that PTV may be a viable method for estimating vortex line density in steady-state thermal counterflow. However, the assumption that G2 track lengths represent the mean free path should be approached with caution. It does not account for the possibility of a mean vortex tangle drift, an effect which is difficult to predict due to limited

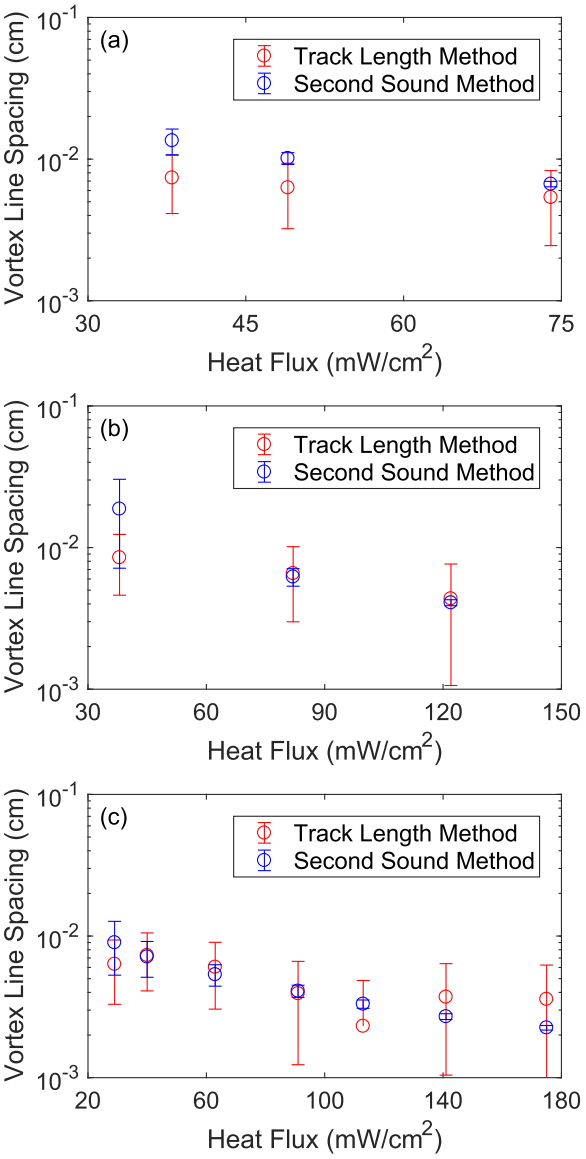

FIG. 3. Prediction of mean vortex line spacing using G2 mean free path model and traditional second sound attenuation for (a) $T = 1.70$ K, (b) $T = 1.85$ K, and (c) $T = 2.00$ K.

understanding. The true mean free path might be given as $s = s_p(1 - C)$, where s_p represents the observed mean free path of the particles (i.e., the mean length of the longest 10% of observed G2 tracks), and $C = v_L/v_n$ is a correction factor relating the mean vortex tangle drift velocity v_L to the normal fluid velocity. Several experiments suggest that v_L is similar to v_s for small enough heat flux [15,20,25,26]. We therefore constrain $C > v_s/v_n$, or equivalently, through conservation of mass, $C > -\rho_n/\rho_s$. It has also been reported that the tangle may drift in the same direction as the normal fluid when the heat flux is larger [27].

Disparity among existing experiments makes it difficult to define a precise value for C, but we can infer the following picture. For counterflow driven by small heat flux, when $v_L \approx v_s$ [15,20,25,26], $C \approx -\rho_n/\rho_s$ and a correction factor of ρ/ρ_s should be applied to Eq. (1). This may improve

agreement between the curves shown in Fig. 3 for low heat flux. For higher heat flux, when $v_L \ll v_n$ [25,28], $C \approx 0$, which is consistent with the agreement shown in Fig. 3 between line spacing measured by second sound attenuation and the mean free path model for higher heat flux.

Subject to these minor corrections, the mean free path model shows strong validity as an alternative to second sound attenuation for estimation of vortex line density in steady-state thermal counterflow. Since PTV provides spatially resolved velocity measurements, this tool makes localized measurements of vortex line density possible.

IV. EXPERIMENTAL MEASUREMENT OF c_2

In our recent paper, we showed that streamwise and transverse G1 velocity fluctuations σ_{G1} as functions of counterflow velocity $v_{ns} = |v_n| + |v_s|$ can be fit remarkably well by the anticipated root mean square vortex line velocity fluctuations $\langle v_L^2 \rangle^{1/2}$ [20]. Based on local self-induced vortex motion, $\langle v_L^2 \rangle^{1/2}$ is given by

$$\langle v_L^2 \rangle^{1/2} \approx \frac{\kappa c_2 \gamma}{4\pi} \ln\left(\frac{\ell}{\xi_0}\right)\left(\frac{\rho}{\rho_s} v_n - v_0\right) \tag{2}$$

provided the counterflow velocity $\rho v_n/\rho_s$ exceeds a small critical velocity v_0. To illustrate agreement with σ_{G1}, we computed $\langle v_L^2 \rangle^{1/2}$ using values for γ (a temperature-dependent parameter relating L to v_{ns}), v_0, and the parameter c_2 reported in the recent work of Gao *et al.* [29,30], and we approximated the mean vortex line spacing $\ell = L^{-1/2}$ across the entire parameter space. Since the agreement between streamwise and transverse σ_{G1} and $\langle v_L^2 \rangle^{1/2}$ appeared to be reasonable, we can use measured G1 velocity fluctuations to represent $\langle v_L^2 \rangle^{1/2}$, and apply Eq. (2) to estimate c_2. This parameter was introduced as a temperature-dependent coefficient relating vortex line density to the mean square line curvature, $\langle s''^2 \rangle = c_2^2 L$ [31], and has received recent attention for its role in vortex line dynamics.

The parameter c_2 can also be used to describe both the buildup [32] and decay [21] of quantum turbulence. Recent numerical simulations and experiments suggest that, besides temperature, c_2 may depend on the specific flow geometry [30] and vary spatially with local vortex line density [32], which should exhibit spatial variation on the order of flow channel size for a steady-state counterflow with laminar normal fluid. Since estimation of spatially dependent c_2 is still very challenging for numerical simulations [30], and the traditional second sound method provides averaged information across the measurement volume, application of PTV to make whole-field measurements of G1 velocity fluctuations offers a unique opportunity to investigate the spatial dependence of c_2.

To demonstrate estimation of c_2 using experimental G1 particle data, we use Eq. (2) to calculate its average value across the imaging plane. We begin by obtaining values for ℓ, γ, and v_0 using our own apparatus, employing both flow visualization and second sound attenuation according to the procedures outlined by Gao *et al.* [29]. The results for each temperature are tabulated in Table I. It is unclear why $v_0 < 0$ at 2.00 K.

Values for c_2 can then be obtained using the procedure illustrated in Fig. 4. Panels (a)–(c) show $\sigma_{G1} \ln^{-1}(\ell/\xi_0)$ as a function of $v_{ns} - v_0$ for $T = 1.70$, 1.85, and 2.00 K, respectively. The dashed lines represent linear fits for which, according to Eq. (2), the slope is $\kappa\gamma c_2/4\pi$. Values for c_2 that

TABLE I. Measured values for the γ coefficient and v_0.

T (K)	γ (s/cm^2)	v_0 (cm/s)	c_2
1.70	178.6 ± 42.3	0.134 ± 0.135	0.835 ± 0.239
1.85	236.7 ± 22.5	0.109 ± 0.062	0.563 ± 0.103
2.00	277.6 ± 11.0	-0.160 ± 0.038	0.501 ± 0.077

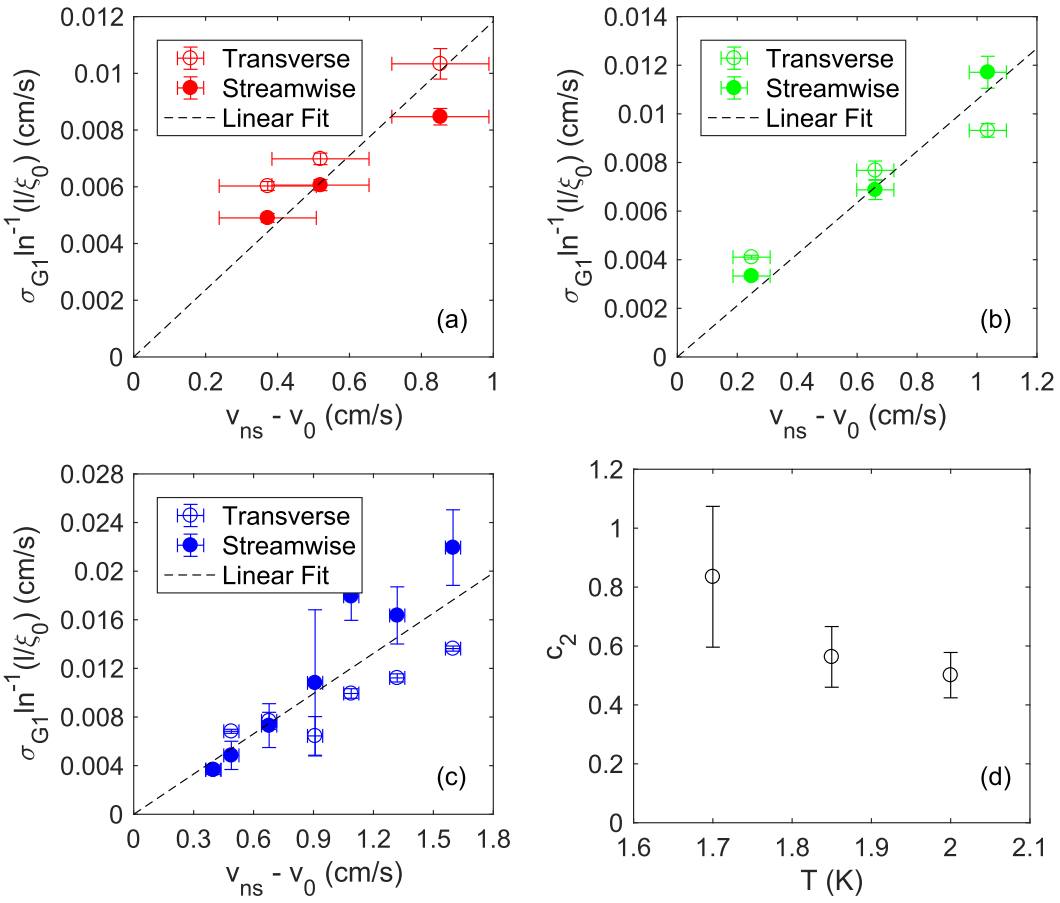

FIG. 4. Linear fit to $\sigma_{G1} \ln^{-1}(\ell/\xi_0)$ as a function of $v_{ns} - v_0$ at (a) $T = 1.70$, (b) 1.85, and (c) 2.00 K. (d) Extracted values of c_2 as a function of temperature.

produce the lines are shown in Fig. 4(d) and tabulated in Table I. They are slightly less than those reported in existing simulations [30,31] and experiments [32], but the overall trend, a decrease with increasing temperature, is preserved. Geometric factors, i.e., the relatively large size of the experimental flow channel, may be partially responsible for the difference. It should also be kept in mind that while fluctuations of the local vortex line velocity play a large role in G1 velocity fluctuations [20], they are not solely responsible. Other factors, such as drag from the normal fluid, can also affect the G1 particle velocity [7,8]. Nonetheless, the results indicate that use of PTV to estimate c_2 is indeed feasible, implying that the parameter can be spatially resolved by estimating its local value based on local G1 velocity fluctuations.

V. VORTEX RECONNECTION AND VELOCITY PDF TAILS

Transverse velocity u_p PDFs for solidified particles tracing thermal counterflow typically exhibit a classical Gaussian core with $|u_p|^{-3}$ power-law tails [16,33]. Recently, we applied our separation scheme to reveal that these tails can be attributed to G1 [20]. Naturally, one might wonder what occurs in the superfluid and vortex tangle that results in G1 particle velocity PDFs with this structure.

Interestingly, it has been shown that PDFs for two physical mechanisms also exhibit these same power-law tails. One is the PDF for a velocity field in the vicinity of a singular vortex, which is proportional to $|v|^{-3}$ for large values of the velocity, i.e., in the tail region [34,35]. Therefore,

the PDF for v_s in the vicinity of a quantized vortex should exhibit the power-law tails. This phenomenon has been demonstrated by numerical simulations [36], and has been invoked to explain the observation of power-law tails in transverse particle velocity u_p PDFs [16,17]. We note in passing, however, that local pressure gradients in the vicinity of a vortex line tend to pull particles into the vortex core, rather than cause them to trace the superfluid velocity field [35,37,38].

Alternatively, when two vortices approach, reconnect, and separate from each other, the minimum separation distance δ grows in time as $\delta \propto |t - t_0|^{1/2}$, where t_0 is the time at which the reconnection occurs [33,39,40]. The separation velocity is then proportional to $|t - t_0|^{-1/2}$, and the PDF should also take a form proportional to $|v|^{-3}$. Since particles have a tendency to become trapped on vortices, this scaling should be reflected in the observed motion of trapped particles and their corresponding velocity PDFs. Indeed, Paoletti *et al.* have shown through visualization of decaying counterflow that particle velocity PDFs take the form $|v|^{-3}$, and they identified numerous pairs of particles moving away from each other with the separation distance growing proportionally to $|t - t_0|^{1/2}$ [33]. This is certainly a convincing link between vortex reconnection and velocity PDF power-law tails, but no direct link was established between these pairs of particles and the tail region of the PDF.

With the separation scheme, a direct link can be established by analyzing the kinematics of particles that exhibit G1 behavior *and* contribute to the transverse PDF tail region. Since our data come from steady-state counterflow, acceleration along the tracks must be considered to remove effects of the mean flow. Based on the $\delta \propto |t - t_0|^{1/2}$ scaling, acceleration along tracks containing a vortex reconnection should be proportional to $|t - t_0|^{-3/2}$.

We first identify G1 tracks containing a segment that contributes to the G1 transverse velocity PDF tail region, which we define as $|u_p| > \mu_{u_p} + 4\sigma_{u_p}$ (see Fig. 2). Figures 5(a)–5(c) show an example of these G1 tracks at each temperature, with the first point in each track indicated by a blue circle. In each of these tracks, the high velocity segment (indicated by the arrow) is accompanied by a strong acceleration and deceleration as well as a noticeable change in direction. These characteristics are indicative of vortex reconnection.

As a first approximation, we assume that reconnection occurs midway through the track segment that contributes to the PDF tail. It follows that the beginning of the identified segment occurs at $t = t_0 - dt/2$, and the end of the segment occurs at $t = t_0 + dt/2$, where dt is the image acquisition interval. We can then calculate acceleration along each track away from (forward event) and towards (reverse event) [33] the reconnection site as a function of elapsed time, and fit the acceleration magnitude $\|\mathbf{a}\|$ for each candidate track with a power-law curve of the form

$$\|\mathbf{a}\| = C|t - t_0|^{-3/2}, \tag{3}$$

where C is the fitting parameter. Figures 5(d)–5(f) show the acceleration magnitudes along each of the corresponding tracks in Figs. 5(a)–5(c). Forward events are shown in blue and reverse events in red, and the dashed line represents Eq. (3). In all three cases, acceleration along the track agrees remarkably well with the predicted $|t - t_0|^{-3/2}$ scaling. Interestingly, the fitting parameter is approximately the same in all three cases, having an average value of $C \approx 0.25$ mm/s$^{1/2}$ independent of temperature. This provides a positive link between transverse velocity PDF tails and vortex reconnection, since the G1 tracks that contribute to the tails obey the acceleration scaling extrapolated from the work of Paoletti *et al.* [33].

VI. CONCLUSION

Our separation scheme for separately analyzing particles entrained by the normal fluid and those trapped on quantized vortices has led to three noteworthy observations. A simple but remarkably accurate model for the mean free path of particles traveling through the vortex tangle relates G2 track length to mean vortex line spacing, providing a new way to estimate localized vortex line density in steady-state thermal counterflow. G1 velocity fluctuations have been used to estimate the value of c_2, an important parameter related to dissipation of turbulent energy in He II, using a flow

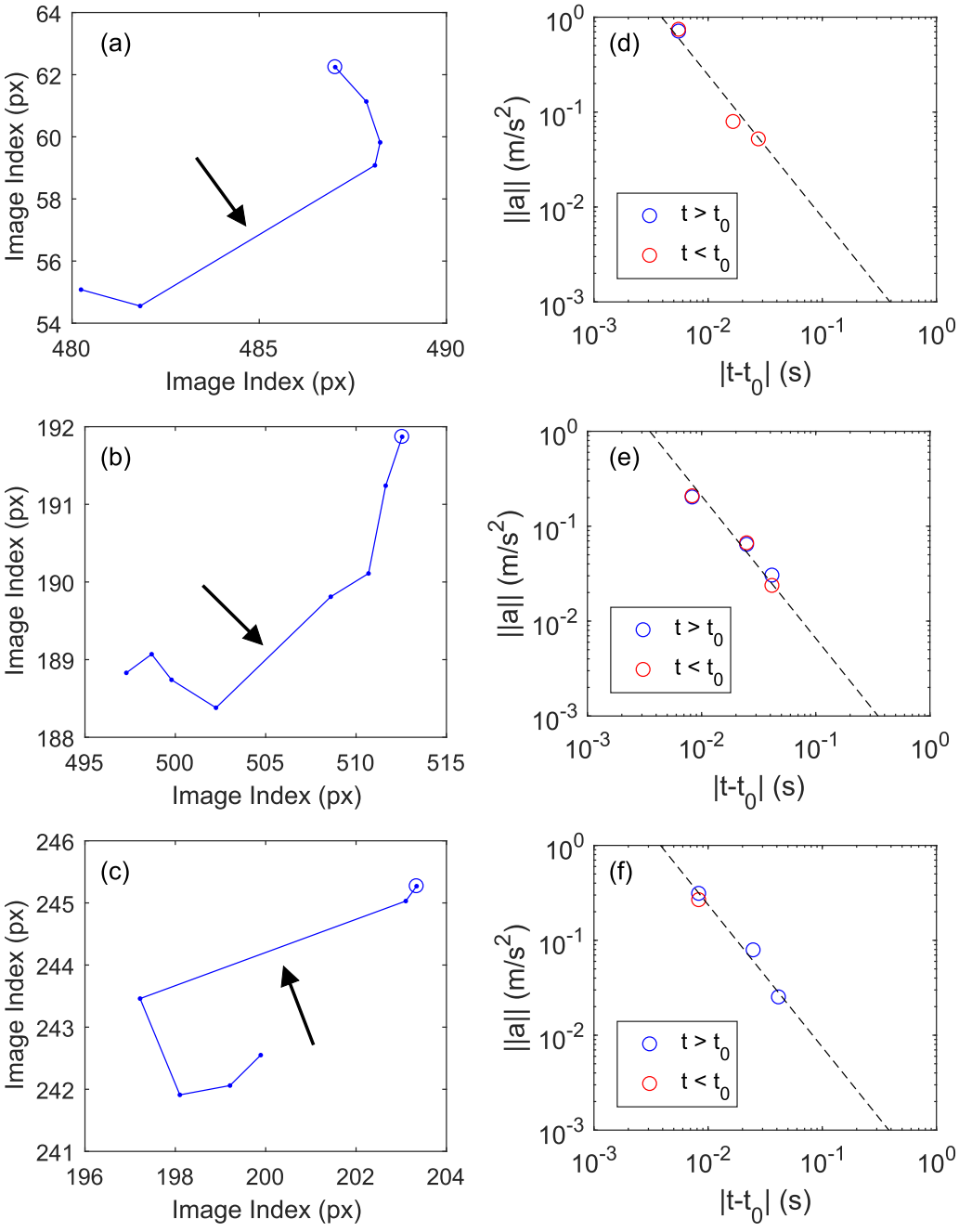

FIG. 5. Selected G1 tracks that contribute to transverse PDF tails at (a) 1.70 K, (b) 1.85 K, and (c) 2.00 K. Blue circles indicate the beginning of each track and black arrows indicate the segment that contributes to the transverse velocity PDF tail. (d)–(f) Corresponding acceleration along the tracks. Dashed lines represent Eq. (3).

visualization method that allows spatial resolution. Finally, vortex reconnection has been positively linked to particle velocity PDF power-law tails by showing that acceleration along G1 tracks that contribute to the tails follows the predicted scaling for vortices accelerating away from (or towards)

a reconnection site. Together, these observation indicate that with an appropriate approach to data analysis, i.e., our separation scheme, PTV is indeed a useful utility for quantifying characteristics of the vortex tangle in steady thermal counterflow.

ACKNOWLEDGMENTS

This work was supported by US Department of Energy Grant No. DE-FG02-96ER40952. It was conducted at the National High Magnetic Field Laboratory, which was supported by NSF Grants No. DMR-1157490 and No. DMR-1644779 and the State of Florida.

[1] W. Guo, M. La Mantia, D. P. Lathrop, and S. W. Van Sciver, Visualization of two-fluid flows of superfluid helium-4, Proc. Natl. Acad. Sci. USA **111**, 4653 (2014).
[2] L. Tisza, Transport phenomena in helium II, Nature (London) **141**, 913 (1938).
[3] L. Landau, Theory of the superfluidity of helium II, Phys. Rev. **60**, 356 (1941).
[4] Y. A. Sergeev and C. F. Barenghi, Particles-vortex interactions and flow visualization in ^{4}He, J. Low Temp. Phys. **157**, 429 (2009).
[5] P. E. Parks and R. J. Donnelly, Radii of Positive and Negative Ions in Helium II, Phys. Rev. Lett. **16**, 45 (1966).
[6] G. P. Bewley, D. P. Lathrop, and K. R. Sreenivasan, Superfluid helium: Visualization of quantized vortices, Nature (London) **441**, 588 (2006).
[7] D. Kivotides, Normal-fluid velocity measurement and superfluid vortex detection in thermal counterflow turbulence, Phys. Rev. B **78**, 224501 (2008).
[8] Y. Mineda, M. Tsubota, Y. A. Sergeev, C. F. Barenghi, and W. F. Vinen, Velocity distributions of tracer particles in thermal counterflow in superfluid ^{4}He, Phys. Rev. B **87**, 174508 (2013).
[9] A. Marakov, J. Gao, W. Guo, S. W. Van Sciver, G. G. Ihas, D. N. McKinsey, and W. F. Vinen, Visualization of the normal-fluid turbulence in counterflowing superfluid ^{4}He, Phys. Rev. B **91**, 094503 (2015).
[10] W. F. Vinen, Mutual friction in a heat current in liquid helium II. III. Theory of the mutual friction, Proc. R. Soc. London, Ser. A **242**, 493 (1957).
[11] H. E. Hall and W. F. Vinen, The rotation of liquid helium II II. The theory of mutual friction in uniformly rotating helium II, Proc. R. Soc. London, Ser. A **238**, 215 (1956).
[12] W. Guo, D. N. McKinsey, A. Marakov, K. J. Thompson, G. G. Ihas, and W. F. Vinen, Visualization technique for determining the structure functions of normal-fluid turbulence in superfluid helium-4, J. Low Temp. Phys. **171**, 497 (2013).
[13] W. F. Vinen, Quantum turbulence: Aspects of visualization and homogeneous turbulence, J. Low Temp. Phys. **175**, 305 (2014).
[14] J. Gao, A. Marakov, W. Guo, B. T. Pawlowski, S. W. Van Sciver, G. G. Ihas, D. N. McKinsey, and W. F. Vinen, Producing and imaging a thin line of He_2^* molecular tracers in helium-4, Rev. Sci. Instrum. **86**, 093904 (2015).
[15] T. V. Chagovets and S. W. Van Sciver, A study of thermal counterflow using particle tracking velocimetry, Phys. Fluids **23**, 107102 (2011).
[16] M. La Mantia and L. Skrbek, Quantum, or classical turbulence? Europhys. Lett. **105**, 46002 (2014).
[17] M. La Mantia and L. Skrbek, Quantum turbulence visualized by particle dynamics, Phys. Rev. B **90**, 014519 (2014).
[18] Y. A. Sergeev, C. F. Barenghi, and D. Kivotides, Motion of micron-size particles in turbulent helium II, Phys. Rev. B **74**, 184506 (2006).
[19] D. Kivotides, Motion of a spherical solid particle in thermal counterflow turbulence, Phys. Rev. B **77**, 174508 (2008).
[20] B. Mastracci and W. Guo, Exploration of thermal counterflow in He II using particle tracking velocimetry, Phys. Rev. Fluids **3**, 063304 (2018).

[21] W. F. Vinen and J. J. Niemela, Quantum turbulence, J. Low Temp. Phys. **128**, 167 (2002).
[22] B. Mastracci and W. Guo, An apparatus for generation and quantitative measurement of homogeneous isotropic turbulence in He II, Rev. Sci. Instrum. **89**, 015107 (2018).
[23] I. F. Sbalzarini and P. Koumoutsakos, Feature point tracking and trajectory analysis for video imaging in cell biology, J. Struct. Biol. **151**, 182 (2005).
[24] L. Skrbek and K. R. Sreenivasan, Developed quantum turbulence and its decay, Phys. Fluids **24**, 011301 (2012).
[25] R. T. Wang, C. E. Swanson, and R. J. Donnelly, Anisotropy and drift of a vortex tangle in helium II, Phys. Rev. B **36**, 5240 (1987).
[26] M. S. Paoletti, R. B. Fiorito, K. R. Sreenivasan, and D. P. Lathrop, Visualization of superfluid helium flow, J. Phys. Soc. Jpn. **77**, 111007 (2008).
[27] R. A. Ashton and J. A. Northby, Vortex Velocity in Turbulent He II Counterflow, Phys. Rev. Lett. **35**, 1714 (1975).
[28] D. D. Awschalom, F. P. Milliken, and K. W. Schwarz, Properties of Superfluid Turbulence in a Large Channel, Phys. Rev. Lett. **53**, 1372 (1984).
[29] J. Gao, E. Varga, W. Guo, and W. F. Vinen, Energy spectrum of thermal counterflow turbulence in superfluid helium-4, Phys. Rev. B **96**, 094511 (2017).
[30] J. Gao, W. Guo, S. Yui, M. Tsubota, and W. F. Vinen, Dissipation in quantum turbulence in superfluid ^{4}He above 1 k, Phys. Rev. B **97**, 184518 (2018).
[31] K. W. Schwarz, Three-dimensional vortex dynamics in superfluid ^{4}He: Homogeneous superfluid turbulence, Phys. Rev. B **38**, 2398 (1988).
[32] E. Varga and L. Skrbek, Dynamics of the density of quantized vortex lines in counterflow turbulence: Experimental investigation, Phys. Rev. B **97**, 064507 (2018).
[33] M. S. Paoletti, M. E. Fisher, K. R. Sreenivasan, and D. P. Lathrop, Velocity Statistics Distinguish Quantum Turbulence from Classical Turbulence, Phys. Rev. Lett. **101**, 154501 (2008).
[34] I. A. Min, I. Mezić, and A. Leonard, Lévy stable distributions for velocity and velocity difference in systems of vortex elements, Phys. Fluids **8**, 1169 (1996).
[35] M. S. Paoletti and D. P. Lathrop, Quantum turbulence, Annu. Rev. Condens. Matter Phys. **2**, 213 (2011).
[36] A. C. White, C. F. Barenghi, N. P. Proukakis, A. J. Youd, and D. H. Wacks, Nonclassical Velocity Statistics in a Turbulent Atomic Bose-Einstein Condensate, Phys. Rev. Lett. **104**, 075301 (2010).
[37] C. F. Barenghi, D. Kivotides, and Y. A. Sergeev, Close approach of a spherical particle and a quantised vortex in helium II, J. Low Temp. Phys. **148**, 293 (2007).
[38] D. Kivotides, C. F. Barenghi, and Y. A. Sergeev, Interactions between particles and quantized vortices in superfluid helium, Phys. Rev. B **77**, 014527 (2008).
[39] A. T. A. M. de Waele and R. G. K. M. Aarts, Route to Vortex Reconnection, Phys. Rev. Lett. **72**, 482 (1994).
[40] G. P. Bewley, M. S. Paoletti, K. R. Sreenivasan, and D. P. Lathrop, Characterization of reconnecting vortices in superfluid helium, Proc. Natl. Acad. Sci. USA **105**, 13707 (2008).